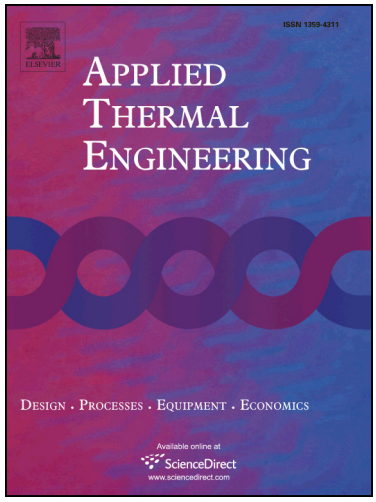

The development of a sub-atmospheric two-phase thermosyphon natural gas preheater using a lumped capacitance model and comparison with experimental results

Hocine Matallah, Will Newton, David James, Ian Cameron, Johann Sienz, Stefan Romocki, Nicholas P. Lavery

PII: S1359-4311(16)30735-9
DOI: http://dx.doi.org/10.1016/j.applthermaleng.2016.05.078
Reference: ATE 8293

To appear in: *Applied Thermal Engineering*

Received Date: 25 November 2015
Revised Date: 11 May 2016
Accepted Date: 13 May 2016

Please cite this article as: H. Matallah, W. Newton, D. James, I. Cameron, J. Sienz, S. Romocki, N.P. Lavery, The development of a sub-atmospheric two-phase thermosyphon natural gas preheater using a lumped capacitance model and comparison with experimental results, *Applied Thermal Engineering* (2016), doi: http://dx.doi.org/10.1016/j.applthermaleng.2016.05.078

The development of a sub-atmospheric two-phase thermosyphon natural gas preheater using a lumped capacitance model and comparison with experimental results

Hocine Matallah[a], Will Newton[a], David James[a], Ian Cameron[a], Johann Sienz[a], Stefan Romocki[b], Nicholas P. Lavery[a]

[a]ASTUTE, Engineering Central, Swansea University Bay Campus, SA1 8EN, UK, h.matallah@swansea.ac.uk

[b]ProHeat, Conwy House, Tawe Business Village, Swansea Enterprise Park, SA7 9LA, UK
sromocki@proheatsystems.com

Abstract The pre-heating of natural gas supplied to both domestic and industrial use is required to counteract the Joule-Thompson effect due to pressure reduction. Most existing pre-heaters are in the form of water bath heaters, where both the burner and exchanger are immersed in a closed water tank. These systems usually have a low efficiency, and as a result of thermal inertia have a long time lag to accommodate changes in Natural Gas (NG) mass flow rates.

In this paper, the two-phase thermosyphon theory is implemented in a sub-atmospheric context to design and study a new preheating system in a transient fashion. This system is partially vacuumed (absolute pressure of 2kPa) to lower the temperature operation range to reduce the required working fluid volume, hence reduce the required energy and improve the response time. The transient numerical model is based on a lumped capacitance method, and the full system is solved by using a fourth order Runge-Kutta method. The numerical model is validated through comparison with experimental results. Minimum efficiency of 68% has been achieved in some tests, whilst maximum efficiency of 80% in other tests.

Simulations of the thermosyphon preheater system have been performed to analyse the effect of changing the working fluid volume and composition.

Keywords: Thermosyphon, Sub-atmospheric, Heat transfer, Joule-Thompson, Lumped-capacitance, Runge-Kutta

1. Introduction

Preheaters are used to heat natural gas prior to reducing compressed flow to ensure no ill effects of the temperature dropping due to the Joule-Thompson effect, such as hydrates forming [1] within the pipe line or valves. If there is any water within the flow, and preheating is not conducted, hydrates can form within the pipes, and build, which can eventually form a plug in the flow.

Within the UK, water bath preheaters are the industry standard, due to a robust and simple design, which has a proven track record; many water baths are still in service after 40 years, but typically last for 25 years. The water bath preheater's

design has a burner and a heat exchanger both submerged in the water bath in a single tank. Water bath preheaters have been shown to have relatively low efficiencies, in the region of 40 – 60 % [2]. The UK has legally committed to reducing the carbon footprint by 80 % by 2050 [3], and with as many as 1,000 preheating sites across the UK that need replacing, this provides an excellent opportunity to replace with more efficient preheaters.

A novel preheating system using thermosyphon technology has been developed and is a good replacement for the water bath heater. Thermosyphons use natural convection cycles to transfer heat from a source to a sink, often, but not always, involving phase change, similar in some respects to heat-pipes with some distinct differences [4], see Fig. 1. Thermosyphons with different designs are used in gas turbine blade cooling, water heaters, cooling systems for nuclear reactors and many other cooling applications.
As shown in Fig. 1, the heat source may be on the lower horizontal or vertical sides and the sink may be located at the upper horizontal or vertical sides, yielding different combinations. In this paper, the source and sink are at the lower and upper horizontal sides, respectively.

Smaller thermosyphons have been the subject of extensive research, particularly experimentally. Lin et al. [5], (1995) focused on geyser boiling in a vertical annular two-phase closed thermosyphon in an experimental study. Geyser boiling is a phenomenon that happens when a large quantity of the working fluid is ejected from the evaporator to the condenser with high velocity, and therefore oscillatory heat transfer behaviour may exist. This may damage the thermosyphon. The effect of many parameters has been taken into account: the heat load, liquid fill in the evaporator and the condenser temperature. Ethanol and water were used as working fluids. Geyser boiling was shown to occur under low and high heat loads, the period of the geyser boiling is shorter for a higher heat load, a smaller liquid fill, and a shorter evaporator length. A correlation equation was proposed as the mean heat transfer coefficient was found to have an almost linear relationship with the heat input in the logarithmic scale. With ethanol as the working fluid, it was found that geyser boiling occurred in a narrower range of the heat load than with water.

Due to the design and large size (order of meters) of the thermosyphon investigated in this work and the high heat load considered (order of 100kW), geyser boiling is considered to have little effect on the heat transfer process. The so-called flooding and entrainment limitations, that are present for small size devices, are avoided. The Ledinegg instability [6] is also assumed to be insignificant as the boiling boundary is far from the tube.

Noie et al [7] (2005) considered experimental investigations on a vertical two-phased closed thermosyphon under vacuum using a closed vertical container. Investigations into parameters such as input heat transfer rates, filling ratio of the working fluid and the evaporator lengths were studied to assess the heat transfer performance. It was concluded that the evaporator section was almost isothermal, and that the temperature at the condenser was lower. When the evaporator length was constant, the temperature decreased with an increase in filling ratio to a critical

value. With an increase in evaporator length, the critical filling ratio decreased. The maximum heat transfer rates occurred at different filling ratios for each evaporator length.

Garrity et al. [8], (2007) employed a small scale two-phase thermosyphon as a cooling system to dissipate the waste heat from proton-exchange membrane (PEM) fuel cells. The maximum heat flux that can be removed from the heated microchannel plate is 32kW/m2. Both experiment and simulation were presented. The thermal hydraulic model proposed was based on the pressure change around the flow loop, using gravity, friction and acceleration. HFE-7100 was used as the working fluid. The prediction of the mass flow rate, pressure drop, and microchannel plate thermal field were found to be satisfactory, and the temperature in the plate wall was between 66 and 82 C.

Jouhara et al [9] (2010) considered the performance of a vertical thermosyphon with four different working fluids; water, FC-84, FC-77 and FC-3283. Seven nucleate pool boiling heat transfer correlations were compared to results from experimentation, and found to be in good agreement when water was used as the working fluid. Maximum heat transport capacity was found to be when water was used as the working fluid, except when considering low operating temperatures. This was due to the saturation temperatures of the other working fluids.

Franco and Filippeschi [10] (2012) conducted a detailed review into existing experimental studies for a small dimension closed loop two-phase thermosyphon. One of the main findings was that the aims for experiments were often different, therefore, the outcomes were different. The result is that no generalised outcomes could be observed. The implication of the lack of generalised results being that the application of closed loop thermosyphons in different operating conditions is hard to achieve. The complexities involved in conducting experimentation due to highly sensitive equipment were shown, often due to the presence of air.

Many experiments have been carried out for small scale thermosyphon, order of millimetres. Franco and Felippeschi [11] (2013) designed an experimental test rig in which they analysed the thermo-fluid dynamic behaviour of CLTPT and in particular the link between heat flow rate and mass flow rate with growing input power ranging approximately from 0 to 1.7kW and operating pressure between 0.1 and 1 bar. The condenser was about 1m above the evaporator. Water and ethanol were used as test fluids. The device had a gravity dominated regime with a reduction in the friction dominant regime. Higher instabilities are observed at higher heat loads at which the mass flow rate is reduced from a maximum value. Operating pressure and filling ratio, as shown, has a big impact on the maximum mass flow rate. There is a recommendation to use water at higher loads than ethanol, to avoid critical conditions in the evaporation zone which may arise leading to the occurrence of a second type of instability.

They described in their review [10] (2012) the conditions that affect the behaviour of the CLTPT but for small dimensions (order of some millimetres). They analysed the disagreements between the experimental data and the conventional theory

developed for an imposed flow rate. They concluded that the fluid flow and the heat transfer mechanisms should be reconsidered in small to micro-channels and should be validated against experiments. In contrast, in large channels in loop thermosyphons, empirical correlations or numerical codes do not take in consideration the effect of flow regime on heat transfer, but preliminary knowledge of the flow pattern such as film flow boiling nucleate boiling and forced convective boiling is necessary. For sub-atmospheric cases, the filling ratio is reported to play an important role.

An experimental study on the performance of a two phase closed loop thermosiphon using different fill ratios of the working fluid was conducted by Chehade et al. [12] (2014). The evaporator and the condenser are connected by two insulated tubes. The maximum heat input is 0.5kW. Optimal fill ratio reported is between 7% and 10%.

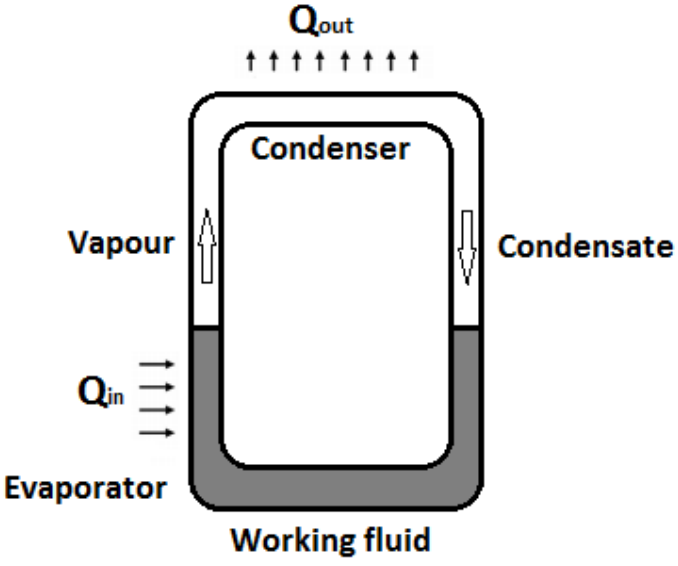

Fig. 1: Diagram of a two phase closed loop thermosyphon

The main benefit of thermosyphons is higher thermal efficiency compared with water baths. They are also simple, with no moving parts required to move the heated working fluid around the system. Due to this, less maintenance is required over the lifetime of the system.

Due to the simple design and high levels of heat transfer, thermosyphons have been the subject of a great deal of research, through experimental techniques [7][9][10] and more recently using computational modelling techniques [13][14][15].

Haider and Joshi [16], (2002) presented an analytical model for the two-phase flow and heat transfer in the closed loop, two-phase thermosyphon (CLTPT). The model

is of small size as the focus is on CLTPTs for electronics cooling. The model is governed by the momentum, energy and mass balances in the system, assuming steady-state conditions and approximating in one-dimensional context. The pressure drops are modelled through the homogeneous two-phase flow model (equal liquid and vapour phase velocities), and all two-phase flow parameters are cross- section averaged, with vapour assumed to be an ideal gas. The friction pressure drop of the two-phase flow imposed by the available gravitational head through the loop is evaluated, and the saturation temperature is predicted from the thermodynamic constraints. The model shown is reported to have good agreement in trends with experimental data for dielectric working fluid PF-5060.

Song [17], (2008) developed an analytical solution for the performance of a typical natural circulation loop, using a typical rectangular shaped natural circulation loop, combining the effects of the frictional pressure drop, the inlet K factor, the geometric parameters, and the system pressure. The analysis predicts the gravity dominated regime and the friction dominated regime. The prediction of the normalised mass flow rate as a function of the heat input, the pressure loss coefficient and the density ratio, are also derived and lead to find an optimal geometric configuration. It was shown that the optimal configuration is barely dependent on the size of the natural circulation loop. The analytical solution proposed may also be extended through a scaling criterion of the ratio of the length scale and the ratio of the heat input.

Milanez and Mantelli [18], (2010) presented an experimental and theoretical study on the effect of pressure drop in the (CLTPT), on the heat transfer limit. When the condensate return level is at the end of the condenser, the heat transfer limit is reached, and any increase in the heat transfer rate yields to a blockage in some parts of the condenser by the condensate and therefore the thermal resistance of the thermosyphon is increased. The theoretical model, based on the pressure drop in both single and two-phase flows, was proposed. The model was validated by a stainless-steel-water prototype, and a good agreement between experiment and the predicted data in the trend was reported, with some under-prediction in the absolute values.

In [19], (2011) Bieliński and Mikielewicz analysed a theoretical one dimensional model that includes mass, momentum and energy balances, invoking empirical correlations for the heat transfer coefficient. Three combinations of the heat source and heat sink positions for the thermosyphon have been studied: Heated from Horizontal side and Cooled from upper Horizontal side (HHCH), Heated from Vertical side and Cooled from Vertical side (HVCV), and Heated from Horizontal side and Cooled from Vertical side (HHCV). They concluded as quoted that “the best choice is dependent on specific technical conditions.” It was shown that for minichannels, an increase of the heat flux leads to an increase of the heat transfer coefficient in flow boiling. In contrast, in the condensation part, the heat transfer coefficient increases with the heat flux reaching a maximum, and decreasing slowly thereafter.

Research into the numerical modelling of heat pipes and thermosyphons has been reported, such as Ferrandi et al. [13], simulating the transient and steady state operation of a sintered heat pipe, using a lumped capacitance method. One has to note that the heat pipe is capillary dominated as opposed to thermosyphons where gravity is dominant, and therefore different equations are solved. They validated their code against previously published data.

The lumped capacitance method was also used by Ziapour and Shaker [14] where they conducted a numerical study on transient and steady state behaviours of a two-phase closed thermosyphon represented by a closed vertical container. A modified Runge-Kutta method was used to enhance the time integration. It was shown that the condenser surface temperature in the steady state case was independent of the convective effects.

Angelo et al. [15] consider the use of a thermosyphon type method to pre-heat natural gas. The evaporator and condenser were split into separate vessels, with connecting pipes. The natural gas runs through a heat exchanger which uses steam as the second phase for heat extraction. Water was used as the working fluid.

The design adopted in the current work is similar to that of Angelo et al. [15], with two fundamental distinctions; the preheater runs at a partial vacuum which was deemed to improve the overall efficiency of the heat transfer, and a water-ethylene glycol mixture is used as the working fluid.

A numerical model has been developed using a transient network lumped capacitance model, which was detailed in [20]. The resulted system is a first order linear differential which is solved by a fourth order Runge-Kutta scheme.

A pilot of the thermosyphon preheater has been manufactured, and will be put into service at a particular site to replace a water bath preheater which is currently in service. Data gathering was conducted on the pilot during the commissioning stages, which provided data for validation of the model. A typical 24 hour load through the site provided by ProHeat Systems, was used to calculate the performance of the thermosyphon preheaters. The water bath as reported [2] highlights the poor efficiencies associated, however, it is to be expected when considering the large mass of working fluid which is heated, in two vessels, where the required power output may be satisfied with one vessel depending on the load. If one vessel was used, the efficiencies would improve, but not by an amount to make it of comparable performance to the thermosyphon.

2. Natural gas preheaters

2.1 Site load profile

To analyse the performance of the thermosyphon a typical 24 hour load cycle for some specific sites was used. As the flow rate through the preheater site changes continuously throughout the day due to demand, the power required to heat the

natural gas also changes. Typical 24 hour load cycles for three sites are shown in Fig. 2, which shows peak gas requirements occur in the morning and evening, before and after the average working day, when consumer demand is highest.

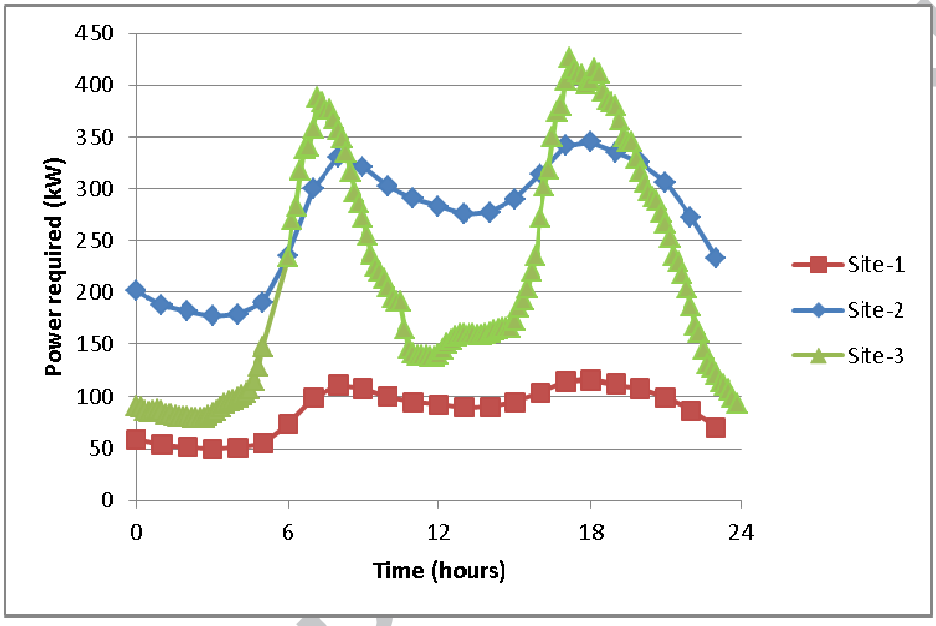

Fig. 2: Sites 1,2 and-3 load data for a 24 hours period

2.2 Water bath preheater

A typical water bath preheater system is shown in Fig. 3, which has been in service for 25 years. The design is simple, with all heat exchange components submerged within the water bath. The flow of the natural gas is split equally between two water bath preheaters at this particular site. Each water bath preheater has a burner rated at 405 kW to meet the peak demands of 330 kW. The reason for two preheaters is that the site always has a throughput of natural gas, therefore there is a need for redundancy at the site, to allow for one of the two preheaters to be serviced whilst the other continues to fulfil the site requirement.

Fig. 3: Water bath preheater

2.3 Thermosyphon preheater

The thermosyphon preheater was designed to have the evaporators and condenser in separate vessels, connected by piping. The evaporator has a burner with a serpentine coil within the bottom half, whilst the condenser has a tightly packed heat exchanger coil. A number of evaporators can be assembled in a parallel configuration to share one condenser depending on power requirements.

The design of the preheater was conducted around the heat transfer required for the natural gas, using a top down calculation method. The maximum volumetric flow of natural gas through a pressure reducing station was the critical design point. This design was focussed on a particular site on a gas distribution network with a bespoke design for specific diurnal and yearly long loading requirements, but the methodology could be adopted to design a system for any site. Each site will have a maximum volumetric flow rate and maximum pressure, and the required pressure and temperature after choke (pressure reduction).

The pilot thermosyphon used for experiments in this paper is shown in Fig. 4.

Fig. 4: Pilot unit - three-burner thermosyphon preheater.

3. Theory

3.1 Thermosyphon Lumped Capacitance Transient Model

Fig. 5 shows the lumped capacitance model in a resistance network form. Convection heat transfer is present between the following parts: burner outer surface and the working fluid, working fluid and inner evaporator chamber, working fluid/evaporated fluid, evaporated fluid and inner evaporator chamber (and transporting-pipes), evaporated fluid and the natural gas (NG) condenser outer surface, and finally, the NG inside pipe surface and the NG-fluid. The conduction heat transfer is represented in the burner and condenser pipes, evaporator and condenser chamber walls, and the fluid transport pipes. The working fluid/evaporated fluids are assumed to have the same temperature.

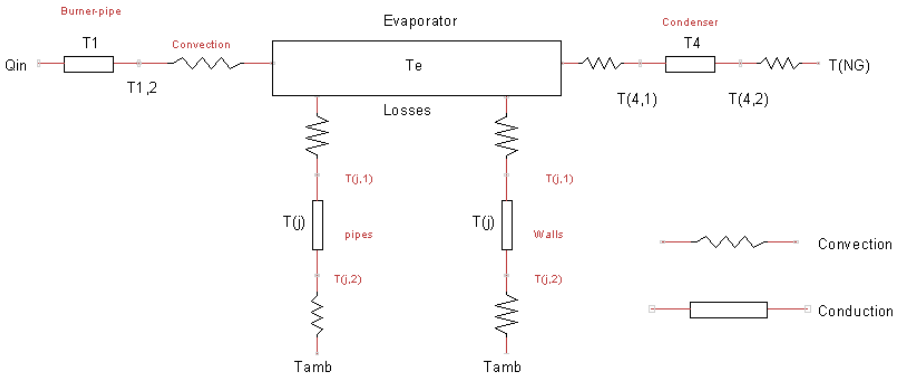

Fig. 5: Schematic diagram of the network model

The input power, $\dot{Q}_{in}$, is assumed as a known quantity and is defined as the power delivered by the combustion of natural gas (already given as in Fig. 2), rather than the calculation of combustion which involves extra equations. The burner pipe temperature, the condenser pipe temperature, the working fluid temperature and the natural gas temperature with extra pipes and wall temperatures were unknown variables to be solved by the network model above.

Considering the input power, $\dot{Q}_{in}$, is given, the burner pipe temperature, T_1, at the middle radius, R_1, is represented by the transient conduction equation as

$$m_1 C_{p1} \frac{\partial T_1}{\partial t} = \dot{Q}_{in} - \frac{2\pi L_1 k_1}{\ln(R_{1o}/R_1)}\left(T_1 - T_{1,2}\right) \quad \textbf{(1)}$$

where $m_1, C_{p1}, k_1, L_1, R_{1o}$ represent the pipe mass, specific heat capacity, conductivity, length and outer radius, respectively. The time is denoted by t. The outer pipe temperature $T_{1,2}$ is defined from the energy balance using conduction (burner pipe)/convection (to working fluid) in function of the evaporator heat transfer coefficient, h_e, by

$$T_{1,2} = \frac{k_1 T_1 + h_e R_{1o} T_e \ln(R_{1o}/R_1)}{k_1 + h_e R_{1o} \ln(R_{1o}/R_1)} \quad \textbf{(2)}$$

Similarly, for the condensation pipe, at the middle radius, R_4, the temperature is given by

$$m_4 C_{p4} \frac{\partial T_4}{\partial t} = -\frac{2\pi L_4 k_4}{\ln(R_{4o}/R_4)}\left(T_{4,1} - T_4\right) - \frac{2\pi L_4 k_4}{\ln(R_4/R_{4i})}\left(T_4 - T_{4,2}\right) \quad \textbf{(3)}$$

The condensation pipe properties are defined in a similar fashion as those of the burner pipe as above, in addition to the inner radius, R_{4i}. From the

convective/conduction energy balance at the outer and inner condenser regions, the temperature $T_{4,1}$ and $T_{4,2}$ are given in the function of the heat transfer coefficient at the condenser outer surface,h_c, and inner surface, h_{NG}, as

$$T_{4,1} = \frac{k_4 T_4 + h_c R_{4o} T_e \ln(R_{4o}/R_4)}{k_4 + h_c R_{4o} \ln(R_{4o}/R_4)};\ T_{4,2} = \frac{k_4 T_4 + h_{NG} R_{4i} T_{NG} \ln(R_4/R_{4i})}{k_4 + h_{NG} R_{4i} \ln(R_4/R_{4i})} \quad (4)$$

The natural gas temperature is represented by T_{NG}.
The natural gas inner surface heat transfer coefficient (h_{NG}) is evaluated for the pipe, with diameter D_h and roughness height ϵ, through the Gnielinski correlation [21]. The Nusselt number is given in as a function of the Reynolds and Prandtl numbers:

$$Nu_{NG} = \frac{(f/8)(Re_{NG} - 1000)Pr}{1 + 12.7(f/8)^{\frac{1}{2}}(Pr^{\frac{2}{3}} - 1)} \quad (5)$$

And the Darcy factor (*f*) is defined as

$$\frac{1}{\sqrt{f}} = -2log_{10}\left(\frac{\epsilon}{3.7D_h} + \frac{2.51}{Re\sqrt{f}}\right) \quad (6)$$

Eq. (6 is solved through non-linear iterative solver.
The $m_1$and m_4 masses of the burner and condenser pipes are defined as a function of the density ρ by

$$m_i = \rho_i \pi (R_{io}^2 - R_{ii}^2) L_i \quad (7)$$

The pool temperature is assumed to be uniform throughout the evaporator boiling domain and is given by

$$m_e C_{pe} N_b \frac{\partial T_e}{\partial t} = \frac{2\pi L_1 k_1}{\ln(R_{1o}/R_1)} N_b (T_1 - T_{1,2}) - \frac{2\pi L_4 k_4}{\ln(R_{4o}/R_4)}(T_{4,1} - T_4) - \sum_{j}^{N-pipes} \frac{2\pi L_j k_j}{\ln(R_j/R_{ji})}(T_{j,1} - T_j) - \sum_{j}^{N-walls} \frac{2A_j k_j}{\lambda_j}(T_{j,1} - T_j) \quad (8)$$

where N_b is the number of burners. The second line in the evaporator equation accounts for pipes and vertical wall losses to the ambient environment. A_j, k_j and λ_j represent the wall (*j*) area, thermal conductivity and thickness. The corresponding temperature for a pipe/wall, j, will be defined in general form as

$$m_j C_{pj} \frac{\partial T_j}{\partial t} = \dot{Q}_{j,1} - \dot{Q}_{j,2} \quad (9)$$

where, for a pipe j,

$$\dot{Q}_{j,1} = \frac{2\pi L_j k_j}{\ln(R_j/R_{ji})}(T_{j,1} - T_j);\ \dot{Q}_{j,2} = \frac{2\pi L_j k_j}{\ln(R_{jo}/R_j)}(T_j - T_{j,2}) \quad (10)$$

for a vertical wall, j,

$$\dot{Q}_{j,1} = \frac{2k_j}{\lambda_j}(T_{j,1} - T_j);\ \dot{Q}_{j,2} = \frac{2k_j}{\lambda_j}(T_j - T_{j,2}) \quad (11)$$

The inner and outer temperatures are defined from the energy balance as

$$T_{j,1} = \frac{k_j T_j + h_{j,in} R_{j,in} T_e \ln(R_j/R_{j,in})}{k_j + h_{j,in} R_{j,in} \ln(R_j/R_{j,in})};\ T_{j,2} = \frac{k_j T_j + h_{j,out} R_{j,out} T_{amb} \ln(R_{j,out}/R_j)}{k_j + h_{j,out} R_{j,out} \ln(R_{j,out}/R_j)};$$
$$T_{j,1} = \frac{2k_j T_j + h_{j,in} T_e \lambda_j}{2k_j + h_{j,in}\lambda_j};\ T_{j,2} = \frac{2k_j T_j + h_{j,out} T_{amb} \lambda_j}{2k_j + h_{j,out}\lambda_j} \quad (12)$$

To complete the set of equations, it is necessary to dynamically evaluate both the evaporator and condenser heat transfer coefficients h_e and h_c respectively. For a cylinder of inner and outer radii R_{in} and R_{out}, h_e may be calculated through a number of correlations, based on the nucleate boiling excess temperature (difference of the surface and the saturation temperatures exceeding 10°C). In this study, Imura correlation [13] is being employed and is given by

$$h_e = 0.32\left(\frac{g^{0.2}\rho_l^{0.65}k_l^{0.3}C_{p,l}^{0.7}(\rho_l - \rho_g)}{\rho_g^{0.25}h_{fg}^{0.4}\mu_l^{0.1}}\right)\left(\frac{P_{sat}}{P_{atm}}\right)^{0.3}\dot{q}^{0.4} \quad (13)$$

P_{sat}, P_{atm}, $\dot{q}$ represent the saturated pressure, the atmospheric pressure and the heat flux, respectively. Concerning the condensation, the dynamic heat transfer for a horizontal tube with diameter D_{ext}, with the assumption that the surface is exposed to saturated steam, is defined from the Nusselt analysis for a laminar regime [14] as

$$h_c = 0.729\left[\frac{g\rho_l(\rho_l - \rho_g)h'_{fg}k_l^3}{\mu_l(T_{sat} - T_s)D_{ext}}\right]^{1/4} \quad (14)$$

where ρ is the density of the working fluid with subscripts l and g corresponding to the liquid and vapour forms respectively, μ_l the dynamic viscosity of the condensate film, k_l the thermal conductivity of the film, D_{ext} is the external diameter of the heat exchanger coil, T_{sat} is the saturation temperature of the working fluid, T_s is the temperature of the pipe outer surface and is calculated as the average of T_{sat} and T_{in}, where T_{in} is the natural gas temperature in. The modified latent heat of vaporisation, h'_{fg}, is calculated as [22][23]

$$h'_{fg} = h_{fg} + \left(0.68\, c_{p,l}(T_{sat} - T_s)\right) \quad \textbf{(15)}$$

The power, $\dot{Q}$, needed to heat the natural gas is calculated from the maximum enthalpy difference between exit, h_{out}, and inlet, h_{in}, using the following equation

$$\dot{Q} = \dot{m}_{NG}(h_{out} - h_{in}) \quad \textbf{(16)}$$

where $\dot{m}_{NG}$ represents the natural gas mass flow rate. The inlet and outlet enthalpies are known quantities from the temperatures and pressures T_{in}, P_{in}, and T_{out}, P_{out} respectively.

The efficiency (η_{NG}) is based on the ratio of the heat delivered to the process fluid (natural gas/water) and the input burner power as shown

$$\boldsymbol{\eta_{NG} = \dot{Q}_{NG}/\dot{Q}_{in}} \quad \textbf{(17)}$$

To compare with experimental data, the output heat rate, $\dot{Q}_{NG}$, is calculated through the following equation

$$\dot{Q}_{NG} = \dot{m}C_p(T_{out} - T_{in}) \quad \textbf{(18)}$$

where T_{out}, T_{in}, $\dot{m}$, and C_p represent the process fluid output and input temperatures, mass flow-rate and specific heat capacity, respectively.

The resulting set of equations are first order linear differential (in time) as shown

$$\frac{\partial T_1}{\partial t} = f(T_1, T_e, h_e)$$
$$\frac{\partial T_e}{\partial t} = f(T_1, T_e, T_4, T_{NG}, h_e, h_c, h_{NG}) \quad \textbf{(19)}$$
$$\frac{\partial T_4}{\partial t} = f(T_4, T_e, T_{NG}, h_c, h_{NG})$$

Which are solved through a fourth order Runge-Kutta method as follows. Each temperature component is incremented in time using a time step (Δt) as:

$$T_i^{n+1} = T_i^n + \frac{\Delta t}{6}(f_1 + 2f_2 + 2f_3 + f_4) \quad \textbf{(20)}$$

$$f_1 = f(t_n, T_i^n, h_i^n)$$
$$f_2 = f\left(t_n + \frac{\Delta t}{2}, T_i^n + \frac{\Delta t}{2} f_1\right)$$
$$f_3 = f\left(t_n + \frac{\Delta t}{2}, T_i^n + \frac{\Delta t}{2} f_2\right) \quad \textbf{(21)}$$
$$f_4 = f(t_n + \Delta t, T_i^n + \Delta t f_3)$$

The heat transfer coefficients ($h_i = h_e \; or \; h_c \; or \; h_{NG}$) and all other material and physical properties and thermodynamics are updated at each time step. The

ethylene glycol mixture with water properties are updated from temperature values as given by Ferrando [24].

4. Pilot Test Data Gathering for Validation of Model

Data was gathered during the commissioning of a pilot thermosyphon preheater. The pilot consisted of three parallel lower horizontal side evaporators connected to an upper horizontal side single condenser through two separate channels, see Fig. 4. The burners in the evaporator chambers are made from stainless steel 304 with a total length of around 15m and a diameter of 6cm placed at the bottom of the chamber in a (parallel structure). Similarly, the condenser tube is made from carbon-steel, and is about 26m long and 16cm diameter. The evaporator and condenser chambers are, respectively, about 1.5m and 4.7m long with diameters of 80cm and 85cm. The whole system is well insulated with a Rockwool insulator that has a low thermal conductivity to minimise any loss. In contrast, the burners and condenser tubes have a high thermal conductivity. The condenser is above the evaporator by about 1m. The tests were conducted using only one of the three evaporators and the remaining two evaporators were sealed off.

A series of tests was conducted where temperature and pressure data was recorded. The locations where data was recorded are shown in Fig. 6 and in Table 1. The pressure was measured inside the evaporator chamber (11), whilst the temperature was measured in the liquid and steam domains (8 and 9). The process fluid temperatures were also measured at both inlet and outlet (1 and 2). The temperature difference in the pipes were measured from the difference of (4-5) and (6-7). Finally, the exhaust temperature was measured at location 10.

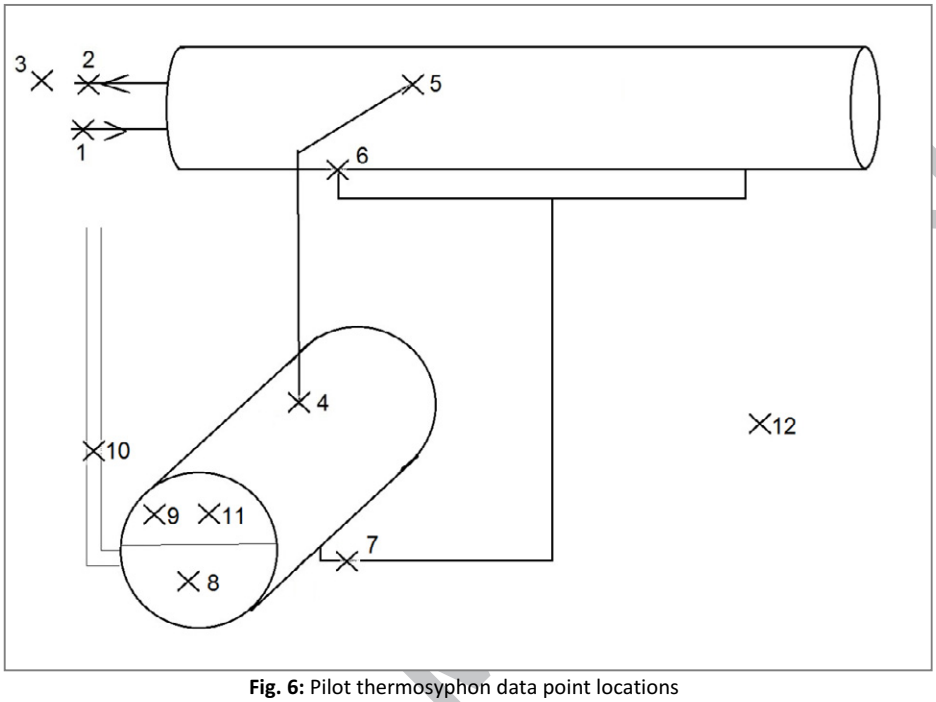

Fig. 6: Pilot thermosyphon data point locations

Table 1. Data points for pilot data gathering.

Name	Data measured
(1) process fluid pipe inlet (externally surface mounted)	Temperature [°C]
(2) process fluid pipe outlet (externally surface mounted)	Temperature [°C]
(3) process fluid outlet (in fluid)	Temperature [°C]
(4) evaporator top/steam pipe inlet (externally surface mounted)	Temperature [°C]
(5) steam pipe exit/condenser (externally surface mounted)	Temperature [°C]
(6) condensate pipe inlet/condenser (externally surface mounted	Temperature [°C]
(7) condensate pipe exit/evaporator bottom (externally surface mounted)	Temperature [°C]
(8) working liquid (internal evaporator)	Temperature [°C]
(9) steam (internal evaporator)	Temperature [°C]
(10) burner exhaust (internal exhaust)	Temperature [°C]
(11) pressure (internal evaporator)	Pressure [Bar(g)]
(12) ambient	Temperature [°C]

The tests were conducted with a working fluid consisting of a 70:30 water-ethylene glycol mixture. The pressure within the system was reduced to an absolute pressure of 2 kPa prior to commencing any of the tests. The process fluid used for the tests was water (in place of natural gas). The inlet temperature is measured

and is about 6°C, and the flow is measured at pipe exit and it is constant with a mass flow rate of 0.42 kg/s.

During the tests the burner on and off periods were controlled manually. The fill volume inside the pilot was varied across two tests. For steady power tests, the power was manually turned on and remained on until the working fluid reached a critical temperature of 90 °C, upon which the burner cycled on-off automatically to keep the working fluid at the critical temperature, before the burner was turned off manually. The tests are listed in Table 2.

Table 2. (**site 2**) unit tests conducted

Name	Power	Fill level (Litre)
Test 1	4 min. on / 4 min. off	255
Test 2	4 min. on / 4 min. off	455
Test 3	Steady	255

After calibration of the system, the uncertainty in the temperature measurement is ±1°C in the range of interest. The uncertainty of the mass flow rate at the condenser pipe exit was found to be ±0.05g/s.

5. Results

5.1 Validation of Model

To validate the model, simulations were conducted to replicate the tests outlined in section 4. In this study, the thermosyphon burner stack-losses are known and given by the manufacturer as 2%, and were taken into consideration in the simulations unless otherwise stated. Therefore, the combustion equation is not implemented.

The first test to be considered was a cycling of the burner on for 4 minutes and off for 4 minutes for a total duration of 36 minutes with an evaporator working fluid fill level of 255 litres (38%).

The transient temperature was monitored at different points as previously discussed and data is shown in Fig. 7, where comparison between simulation and experiment is performed. The working fluid and the process fluid temperatures are compared for many scaling factors of the heat transfer coefficients that relate to the burner wall-working fluid interface (he) and the water pipe wall-heated water (hc). Firstly, no scaling was conducted for he and hc, as displayed in Fig. 7 (hesf=1 and hcsf=1), and the simulation yielded an over estimation of about 15 and 9 degrees Celsius for the working fluid and the process fluid (water), respectively. In contrast, by changing hcsf to 1.7, the working fluid temperature is well predicted, whilst the process fluid temperature is still over predicted by roughly the same range. The simulated efficiency is over-predicting the experimental data and it is in the range of η_{NG} = 71.91% for (hcsf=1.7) and η_{NG} = 68.98% (hcsf=1) compared to the experimental value of γ_{NG} = 51.29%. In this case, the effect of scaling he is found to be minimal in contrast to the effect of scaling hc. By decreasing the scaling factor hesf to 0.73 and maintaining hcsf to unity, the simulated efficiency is reduced

to about 63.42%. In this case, the simulation of the working fluid temperature still over predicts the experimental value.

Fig. 7: Experimental and simulated temperature data for test 1 (4 minutes on, 4 minutes off, 255 litres).

The reason for the simulations not matching the experimental results precisely may be due to the overall heat transfer coefficient calculation associated with the heat exchanger. The mass flow of the process fluid in the experiments was within the transitional flow regime between laminar and turbulence (Re≈3500) rather than fully turbulent as expected for the flow conditions at the site, when Natural Gas is the process fluid in place of water used in these experiments. The transitional regime always represents a numerical challenge by its nature. In this paper, the Gnielinski correlation [21] is implemented to evaluate the Nusselt number.

In the second test (Test 2), the evaporator working fluid fill-volume was increased (from 255 to 455 litres) and the burner was cycled as for Test 1, i.e. the burner on for 4 minutes and off for 4 minutes for a total duration of 36 minutes. The transient temperatures for the working fluid and the processed fluid are shown in Fig. 8a and Fig. 8b, respectively.

The simulations of Test 2 were conducted using he and hc coefficients which were scaled by 0.73, 0.9, 1 and 0.8, 1, 1.5, 1.7 1.9, 2.1, 2.7, respectively. By varying the he scale factors, the effect on both the working fluid and processed water temperatures is minimal (curves overlapping each other in Fig. 8). By fixing the he-scaling and increasing the hc-scaling, the simulated working fluid temperature is decreased and underestimates the temperature of the working fluid recorded experimentally, due to more heat energy being transferred to the processed water for which the temperature is increased and the underestimation is reduced (4 to 10 degrees, instead of 9 to 10 degrees).

a) working fluid

b) process fluid

Fig. 8: Experimental and simulated temperature data for test 2 (4 minutes on, 4 minutes off, 455 litres); a) working fluid and b) process fluid.

Fig. 9: Experimental and simulated temperature data for test 3 (steady power, 255 litres).

Test 3 considered steady power of the burner until the critical temperature of the working fluid had been reached with a fill volume of 255 litres. The transient temperature data is shown in Fig. 9.

A set of h_c scale values, 2.1, 3.1 and 3.3, was used to correlate the simulations to the experimental data. As observed before, the working fluid temperature was in agreement with the experimental counterpart for an h_c scale of 3.3. Again, the heated water temperature first overestimated, and then underestimated by about 20 °C.

The difference between experimental and numerical data is clear in the shape of curvature or concave nature of the differential equation that are of logarithmic type with and without source terms. The type of burner may be simulated with the combustion related equations to mimic the true start-up conditions. Another reason that may affect the simulation is the lack of pressure equation that will dictate the rapid change from cold working fluid to hot/steam. In contrast, in the previous two tests, the working fluid starting temperature was around 40°C.

Numerical models of this type do not typically simulate transient start-up periods well. For this reason further simulations are of sufficient time beyond the start-up period that it does not dominate the results.

Fig. 10 shows an efficiency comparison between the simulations and experiments for the three test cases studied. The simulated efficiency compare reasonably well with the experimental values for Test 3 (steady case). In contrast, for the first two tests, the simulated efficiency is 38% and 11% different or higher/lower from/to the experimental efficiency for Test 1 and Test 2, respectively. This shows that Test 2 (with high fill-volume 68%) is more realistically simulated than Test 1 (fill-volume 38%).

Fig. 10: Efficiency chart comparison between experiment and simulation for studied test cases

5.2 Analysis of thermosyphon performance using actual site data

After validating the transient numerical model using water as the process fluid, for all other simulations presented natural gas is used as the process fluid. To show the benefit of the thermosyphon heater, it was necessary to simulate typical 24 hour loads for actual sites. The thermosyphon system is intended to heat the entire natural gas load with a single or multiple evaporator/burner system. Systems at three sites have been simulated using typical 24 hour load profiles for each site.

To simulate the thermosyphon for the 24 hour cycle, the control of the system was set so that the burner was kept on until the outlet temperature of the natural gas reached the required temperature. Once the temperature was reached, the burner was switched on and off as required to achieve the required output temperature of the natural gas. This simulates the way the actual thermosyphon control will be set to operate.

The preheaters at site normally have process fluid continuously flowing through and are in constant use, therefore, the warm up period will only occur very infrequently as a preheater is brought back into service and is therefore not the period of most interest. Therefore, the initial heating period is not taken into the calculation of efficiency. To compare between sites, an average efficiency for the 24 hour loads is evaluated. This average efficiency is calculated as the ratio of the total heat energy delivered into the heated natural gas to the total heat energy used by the burners over the total period of time.

Furthermore, it was necessary to check the evaporation and condensing scaling factors developed in the validation process above. For site 1, the effect of the working fluid composition and different working fluid evaporator fill levels are also analysed. For sites 2 and 3, the water/ethylene glycol mixture is taken as 70/30 as for the experiments and likely to be the actual composition required to prevent freezing. The effect of scaling the evaporator heat transfer coefficient, h_e, was evaluated for scale factors of unity and 0.73 (as used in the simulation validation, where water was used as the process fluid).These scale factors show little effect on the outcome, hence a value of unity is chosen. In contrast, the process fluid was changed from water to natural gas, where it affected the internal heat transfer coefficient correction due to smooth/rough pipe and flow effects. In the reported experiments with water as the process fluid, the Reynolds number was approximately 3600 (the Prandtl number is approximately 7.2) and the regime represents a transition between laminar (Re<2300) and turbulent flows (Re>4000) [11]. In this case, laminar and turbulent flows were possible and depend on other factors, such as flow uniformity and pipe roughness. In contrast, for the natural gas flow, the Reynolds number was around 1 million (10^6), corresponding to a turbulent flow (the Prandtl number is around 0.83). Hence, the scaling for the internal heat transfer coefficient for natural gas as the process fluid is likely to differ from the pilot experiment using water as explained below. The Gnielinski's correlation for turbulent flow in tubes should be valid for this purpose [21].

It is worth noting that the thermosyphon stack-losses are around 2%. These losses were taken into consideration in the simulations unless otherwise stated.

An initial temperature of 6 degrees Celsius was set for the burner, the condenser and the working fluid at the start-up time. The process fluid inlet temperature was 4 degrees C, whilst the outlet temperature was load dependent to ensure it remains above zero after the Joule-Thomson effect which occurs during the subsequent depressurisation.

5.2.1 Effect of water/ ethylene glycol composition of working fluid

Ethylene glycol is added to water to prevent the working fluid freezing during cold weather, if the system is unused. As a consequence, the boiling point is increased monotonically with increasing ethylene glycol percentage, and therefore a high amount of ethylene glycol may need more energy to reach the boiling point in the

thermosyphon. Hence, an optimised composition is needed for a good combination between freezing and boiling points of the working fluid.

To study the effect of water/ethylene glycol ratio on efficiency, load profile data for one site (Site-3) for a period of 24 hours was used see Fig. 2. In this site data, two peak demand periods occur when the demand is much higher than at other times of the day, one during the morning and one during the evening. Two burners are available if necessary with a power of 400kW each (98% efficient) as the highest power needed is about 427kW.

A total of six working fluid evaporator fill levels (38% to 88% with a step of 10%) and 5 ethylene glycol compositions (0%, 10%, 20%, 30% and 50%) are studied for Site 3.

A temperature plot shown in Fig. 11 shows the temperatures at the locations associated with the thermosyphon for a working fluid evaporator fill level of 68%, and a 30% ethylene glycol composition. The temperature was recorded once the starting period finished (around 84 minutes) and the process fluid outlet temperature (T_{NG}) had reached the required output temperature. T_{NG} remains fairly constant thereafter. The burner wall, working fluid and condenser wall temperatures all follow the same trends, which are directly linked to the flow rate of natural gas, and therefore the required power shown in Fig. 2. As mentioned previously, the warm up period for the preheaters in the simulations is not of significant interest and should be ignored when comparing the results.

Fig. 11: Temperature at locations for 24 hour load for the thermosyphon for site 3, 68% fill and 30% ethylene glycol.

Similarly, the dynamic heat transfer coefficients for the evaporation (h_e) and the condenser outer and inner surfaces (h_c and h_{NG}) for site 3 for the 24 hour load profile are shown in Fig. 12. The evaporator heat transfer coefficient (h_e) varies between 1000 *W/m^2.C* and 3300 *W/m^2.C* and depends on the burner being on or off to maintain a constant natural gas output temperature (h_e is not included in the Figure due to its rapidly changing value which would make the Figure difficult to read). In contrast, the condenser outer surface heat transfer coefficient (h_c) is maintained at approximately constant value of 4000 *W/m^2.C* once the output natural gas temperature is constant, whilst the inner surface coefficient changes with the natural gas load, h_{NG} increases with load increase and decreases accordingly (see Fig. 12) following the site 3 plot shown in Fig. 2.

Fig. 12: Heat transfer coefficient for evaporation, condenser outer and inner surfaces for 24 hour load for the thermosyphon for site 3, 68% fill and 30% ethylene glycol.

As expected, the highest efficiency is observed with water (as also reported by Jouhara et al [5]), and decreases with increasing ethylene glycol mixture, as displayed in Fig. 13. This is true for all fill-levels simulated: 38%-88%. An efficiency

loss of 10% is predicted if a ethylene glycol mixture of 50% is used instead of water.

Fig. 13: Effect of working fluid ethylene glycol/water composition on efficiency

5.2.2 Effect of working fluid evaporator fill-level ratio

In this case, the working fluid water/ethylene glycol composition is fixed but the evaporator fill level ratio is varied. As displayed in Fig. 14, for any water/ethylene glycol mixture (0, 10, 20, 30 and 50%), the efficiency barely changes below a fill-ratio of 68%. Beyond this level, the efficiency decreases with increasing fill-ratio by about 3%.

Fig. 14: Effect of filling ratio on efficiency

In summary, the simulations indicate that the highest efficiency is achieved with the lowest fill level and the lowest ethylene glycol concentration.

5.2.3 Other site simulations

The next case studied corresponds to site 1, where a burner input of 120kW was considered with different evaporator fill ratios as before (38% to 88% with a 10% step), and a stack loss of 2% using a ratio of 70/30 for the water/ethylene glycol composition.

The efficiency increases slightly with increasing working fluid fill level ratio, being around 80% for fill ratios of less than 68%, and increasing by about 2% for higher volume fills as displayed in Fig. 15.

In contrast, for the site 2, two burners of 180kW each were utilised. The efficiency in this case barely changes and it is about 70% for all fill level ratios.

Fig. 15: Effect of filling ratio on efficiency for sites 1 to 3

These simulation results comparing the efficiencies at the 3 sites with different evaporator fill ratios indicate that the selection of the optimum fill ratio is dependent on the required load at a particular site.

6. Conclusions

A new preheater has been designed utilising sub-atmospheric two phase thermosyphon theory to replace existing water bath preheaters. A transient numerical model of the thermosyphon has been developed using a lumped capacitance method. In contrast, the proposed model can be programmed and maintained with low cost and can be used as a predictive tool. A 24 hour period has been simulated using data and thermosyphon designs for 3 different sites, and efficiencies are calculated and compared.

Validation of the transient mathematical model of the thermosyphon was performed through comparison with experimental results, and the use of the experimental results to calibrate some of the heat transfer coefficients, particularly the evaporation and natural-gas internal flow heat transfer coefficients.

The simulations predict the experiment in some cases, and under-predict in the worst scenarios, showing that the thermosyphon is fulfilling its duty. The importance of accounting for the correct flow regime (laminar or turbulent) should be noted as it has been shown that this dramatically affects the heat transfer coefficient. Effect of the pipe-roughness is taken into account to calibrate the heat-transfer coefficient.

The limitations of the model clearly indicate that the startup period should be eliminated from the efficiency evaluation. The reason that the start-up period is not well simulated by the model may be due to a number of factors such as: the differential equation needs to incorporate the dynamic combustion process within the simulation; fast pressure change; and the non-uniform heat distribution in the burners,uniform after the transition period.

The thermosyphon model shows better efficiencies than the water bath counterpart. The process fluid outlet temperatures were satisfied with all models.

In the simulations, the thermosyphon shows a fast response time and high level of efficiency. The use of a sub-atmospheric pressure allows vapour to be generated at low temperatures, and due to the high energy levels transferred through the condensation process, a large amount of heat transfer can occur, thus, the efficiency is high.

For a water/ethylene glycol composition of 70/30, using site-1 load data, the simulations predicted the efficiency to be around 80%. In contrast, for site-2, where a two-burner system is used the efficiency is predicted to be around 72%.
For Site-3 (4-burners available on demand) using different water/ethylene glycol mixtures and fill level ratios, the highest efficiency is achieved with the lowest fill level in combination with 100% water, giving an efficiency of around 72%. This is good for summer conditions, however for severe winter weather, one has to take account of the freezing point and therefore, the lowest possible ethylene glycol concentration should be used to prevent freezing, but maximise efficiency. To study the effect of different variations in site loads on the efficiency three sites were analysed. Site 1 efficiency is around 80% for an evaporator fill ratio of 68% or less, and increases with increasing fill ratio above 68%, meanwhile Site 2 efficiency barely changes for different evaporator fill ratios. In contrast, Site-3 efficiency decreases for evaporator fill ratios above 68%. Efficiency barely changes for fill ratios of less than 68% for all sites.

Acknowledgments

The authors would like to acknowledge the support of the Advanced Sustainable Manufacturing Technologies (ASTUTE) project, which is part funded from the EU's European Regional Development Fund through the Welsh European Funding Office, in enabling the research upon which this paper is based. Further information on ASTUTE can be found at www.astutewales.com. The authors would like to thank ProHeat Systems and Scotia Gas Networks for providing input data for models and project support including access to industrial preheat equipment for testing.

7. References

[1] S. Gao, "Investigation of interactions between gas hydrates and several other flow assurance elements," *Energy and Fuels*, vol. 22, no. 5, pp. 3150–3153, 2008.

[2] S. H. Azizi, A. Rashidmardani, and M. R. Andalibi, "Study of Preheating Natural Gas in Gas Pressure Reduction Station by the Flue Gas of Indirect Water Bath Heater," vol. 3, no. 27, pp. 17–22, 2014.

[3] "GOV.UK (Accessed 2014)," 2014. [Online]. Available: https://www.gov.uk/government/policies/reducing-the-uk-s-greenhouse-gas-emissions-by-80-by-2050.

[4] D. Reay and P. Kew, *Heat pipes: Theory, Design and Applications*, 5th Editio. Jordan Hill, GBR: Butterworth-Heinemann, 2006.

[5] T. F. Lin, W. T. Lin, Y. L. Tsay, J. C. Wu, and R. J. Shyu, "Experimental investigation of geyser boiling in an annular two-phase closed thermosyphon," *Int. J. Heat Mass Transf.*, vol. 38, no. 2, pp. 295–307, Jan. 1995.

[6] L. C. Ruspini, C. P. Marcel, and A. Clausse, "Two-phase flow instabilities: A review," *Int. J. Heat Mass Transf.*, vol. 71, pp. 521–548, Apr. 2014.

[7] S. H. Noie, M. H. Kalaei, and M. Khoshnoodi, "EXPERIMENTAL INVESTIGATION OF BOILING AND CONDENSATION HEAT TRANSFER OF A TWO PHASE CLOSED THERMOSYPHON," vol. 18, no. 1, 2005.

[8] P. T. Garrity, J. F. Klausner, and R. Mei, "A Flow Boiling Microchannel Evaporator Plate for Fuel Cell Thermal Management," *Heat Transf. Eng.*, vol. 28, no. 10, pp. 877–884, 2007.

[9] H. Jouhara and A. J. Robinson, "Experimental investigation of small diameter two-phase closed thermosyphons charged with water, FC-84, FC-77 and FC-3283," *Appl. Therm. Eng.*, vol. 30, no. 2–3, pp. 201–211, 2010.

[10] A. Franco and S. Filippeschi, "Closed loop two-phase thermosyphon of small dimensions: A review of the experimental results," *Microgravity Sci. Technol.*, 2012.

[11] A. Franco and S. Filippeschi, "Experimental analysis of Closed Loop Two Phase Thermosyphon (CLTPT) for energy systems," *Exp. Therm. Fluid Sci.*, vol. 51, pp. 302–311, Nov. 2013.

[12] A. A. Chehade, H. Louahlia-Gualous, S. Le Masson, I. Victor, and N. Abouzahab-Damaj, "Experimental investigation of thermosyphon loop thermal performance," *Energy Convers. Manag.*, 2014.

[13] C. Ferrandi, F. Iorizzo, M. Mameli, S. Zinna, and M. Marengo, "Lumped parameter model of sintered heat pipe: Transient numerical analysis and validation," *Appl. Therm. Eng.*, vol. 50, no. 1, pp. 1280–1290, Jan. 2013.

[14] B. M. Ziapour and H. Shaker, “Heat transfer characteristics of a two-phase closed thermosyphon using different working fluids,” *Heat Mass Transf. und Stoffuebertragung*, vol. 46, no. 3, pp. 307–314, 2010.

[15] W. Angelo, M. H. Mantelli, and F. H. Milanez, “Design of a Heater for Natural Gas Stations Assisted By Two-Phase Loop Thermosyphon,” *Design*, 2007.

[16] S. I. Haider, Y. K. Joshi, G. W. Woodruff, and W. Nakayama, “A Natural Circulation Model of the Closed Loop, Two-Phase Thermosyphon for Electronics Cooling,” *J. Heat Transfer*, vol. 124, 2002.

[17] J. Song, “Performance and scaling analysis for a two-phase natural circulation loop,” *Int. Commun. Heat Mass Transf.*, vol. 35, no. 9, pp. 1084–1090, Nov. 2008.

[18] F. H. Milanez and M. B. H. Mantelli, “HEAT TRANSFER LIMIT DUE TO PRESSURE DROP OF A TWO - PHASE LOOP THERMOSYPHON,” *Heat Pipe Sci. Technol. An Int. J.*, vol. 1, no. 3, pp. 237–250, 2010.

[19] H. Bieliski and J. Mikielewicz, “Natural Circulation in Single and Two Phase Thermosyphon Loop with Conventional Tubes and Minichannels,” in *Heat Transfer - Mathematical Modelling, Numerical Methods and Information Technology*, InTech, 2011.

[20] W. Newton, H. Matallah, D. James, I. Cameron, N. P. Lavery, J. Sienz, and S. Romocki, “The development of a sub-atmospheric two-phase thermosyphon natural gas preheater using a lumped capacitance model,” in *International Conference on Sustainable Design and Manufacturing*, 2014.

[21] V. Gnielinski, “New equations for heat and mass transfer in turbulent pipe and channel flow,” *Int. Chem. Eng.*, vol. 16, no. 02, pp. 359–368, 1976.

[22] F. Incropera, D. Dewitt, T. Bergman, and A. Lavine, *Fundamentals of Heat and Mass Transfer*, 6th ed. John Wiley & Sons, 2007.

[23] H. Imura, H. Kusuda, J. Ogata, T. Miyazaki, and N. Sakamoto, “Heat transfer in two-phase closed-type thermosyphons,” *Heat Transf. - Japanese Res.*, vol. 8, pp. 41–53, 1979.

[24] M. Ferrando, “Thermophysical Properties of Brines,” *M. Conde Eng.*, vol. 47, no. s1a, pp. 390–392, 2002.

Fig. 1, Fig. 2, Fig. 3, Fig. 4, Fig. 5, Fig. 6

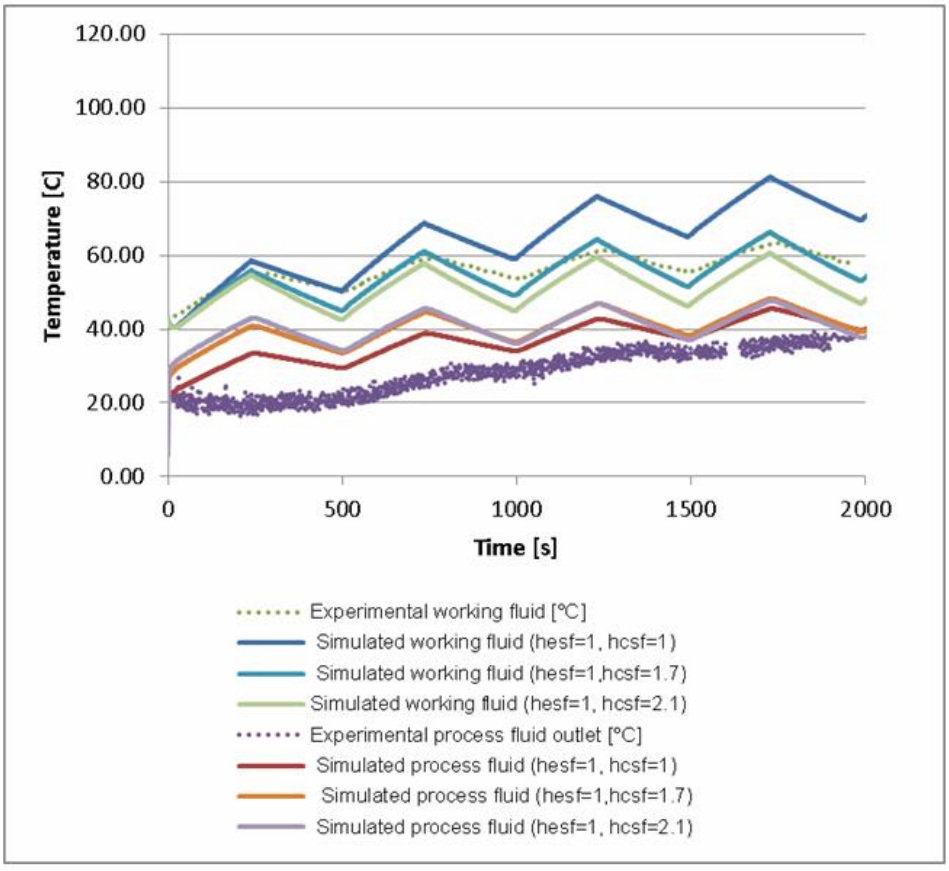

Fig. 7: Experimental and simulated temperature data for test 1 (4 minutes on, 4 minutes off, 255 litres).

Fig. 7:
Legend

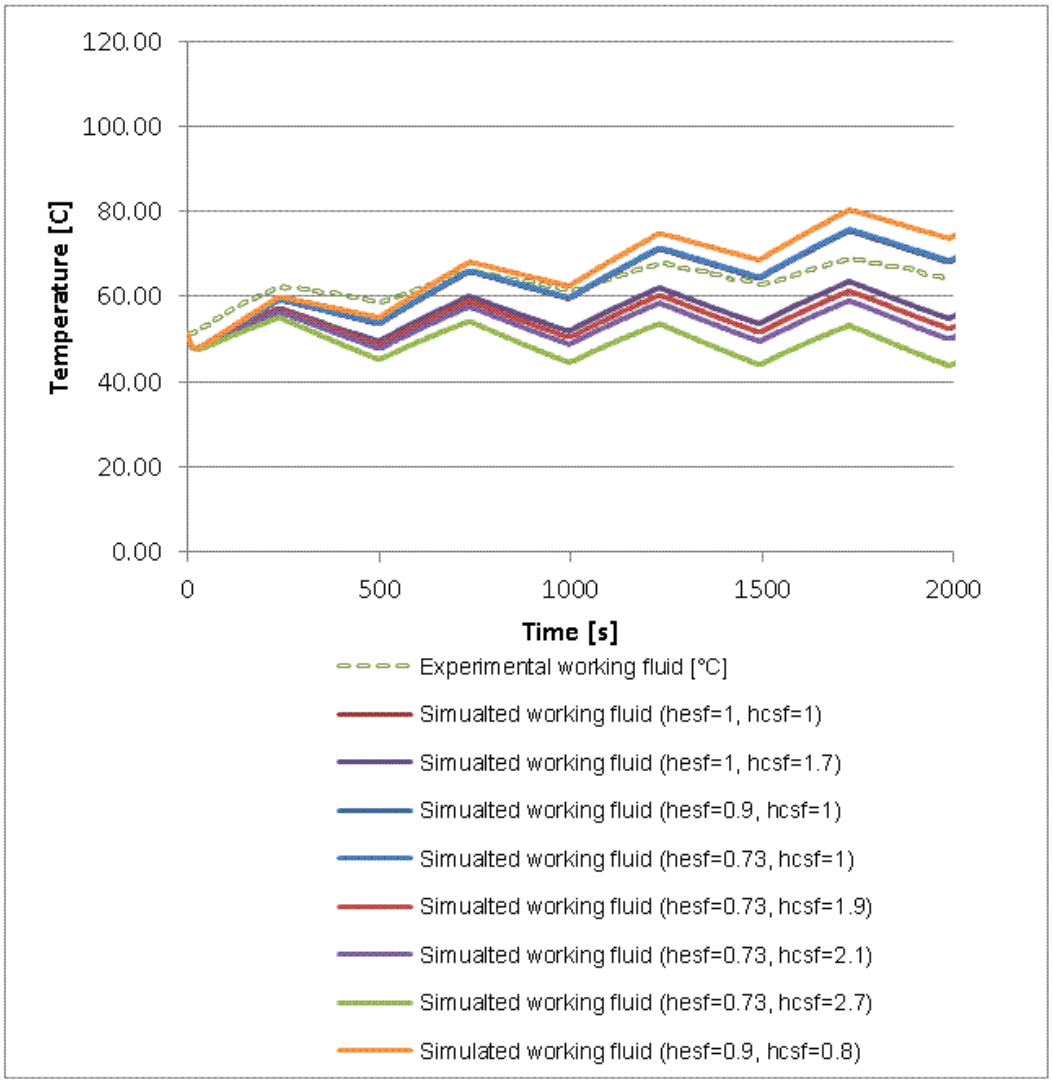

a) working fluid

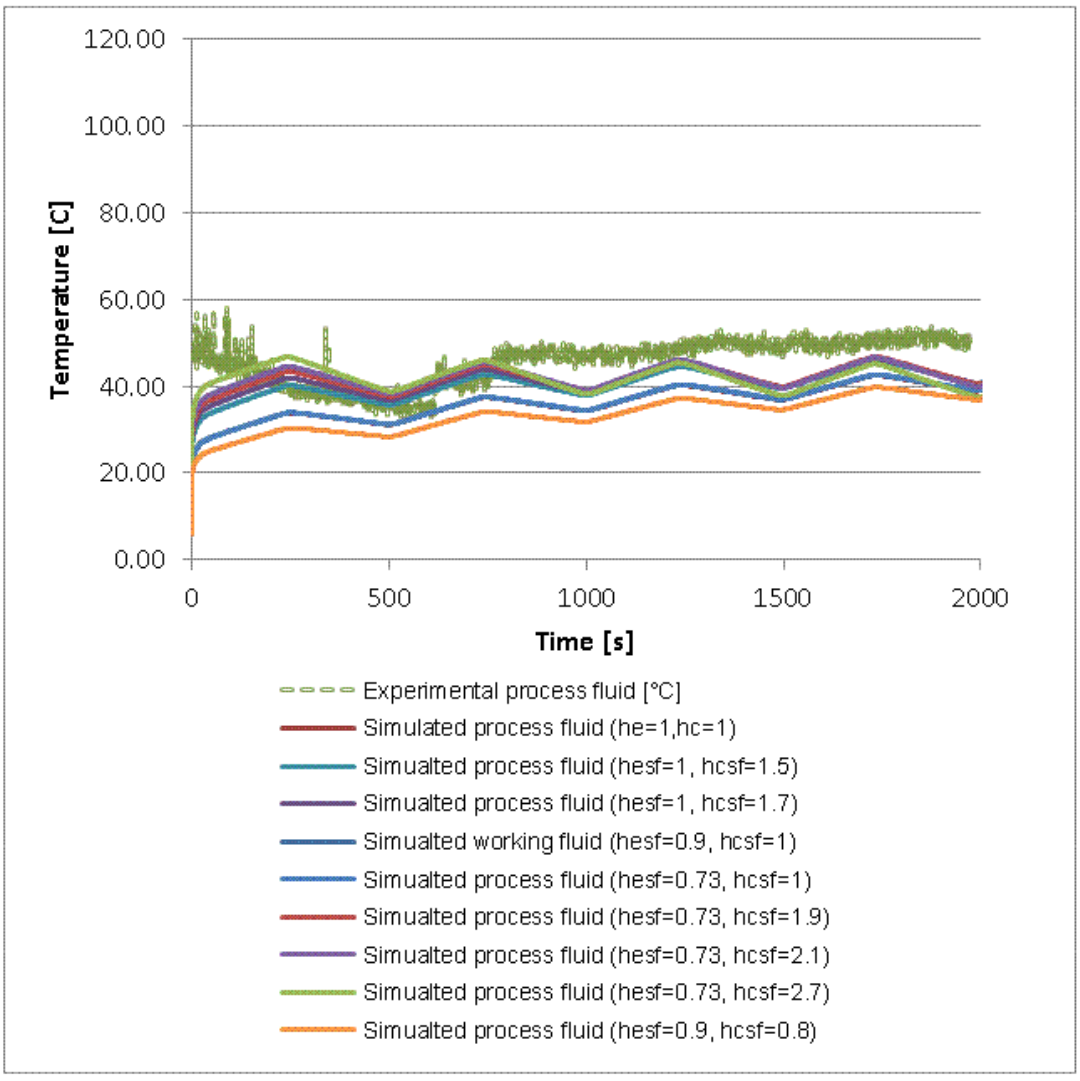

b) process fluid

Fig. 8: **E**xperimental and simulated temperature data for test 2 (4 minutes on, 4 minutes off, 455 litres); a) working fluid and b) process fluid.

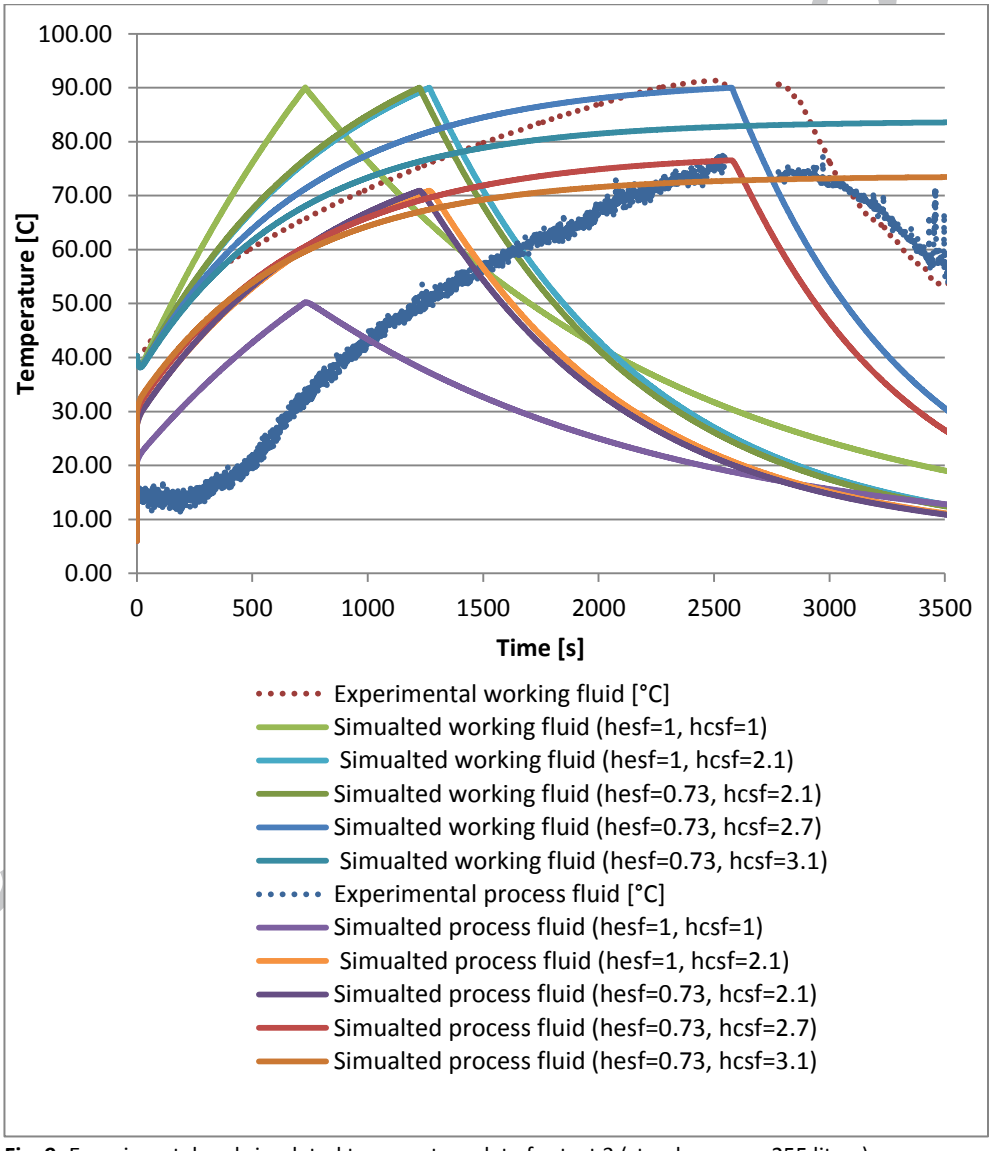

Fig. 9: Experimental and simulated temperature data for test 3 (steady power, 255 litres).

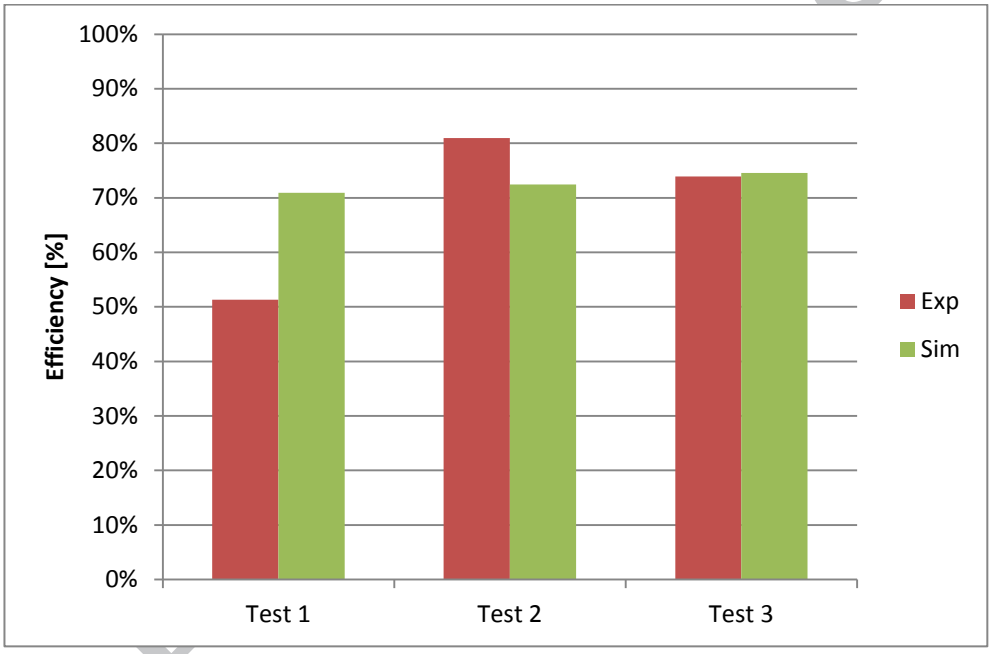

Fig. 10: Efficiency chart comparison between experiment and simulation for studied test cases

Fig. 1, Fig. 2, Fig. 3, Fig. 4, Fig. 5, Fig. 6

Fig. 7:

Fig. 8:

Fig. 9:
Fig. 10:

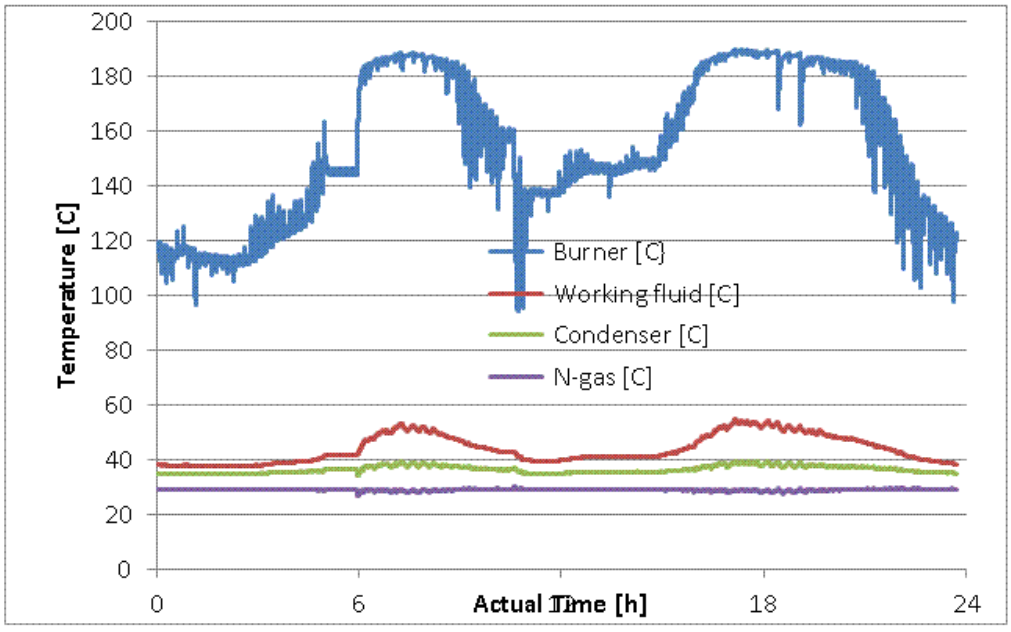

Fig. 11: Temperature at locations for 24 hour load for the thermosyphon for site 3, 68% fill and 30% ethylene glycol.

Fig. 1, Fig. 2, Fig. 3, Fig. 4, Fig. 5, Fig. 6

Fig. 7:

Fig. 8:

Fig. 9:

Fig. 10:

Fig. 11:

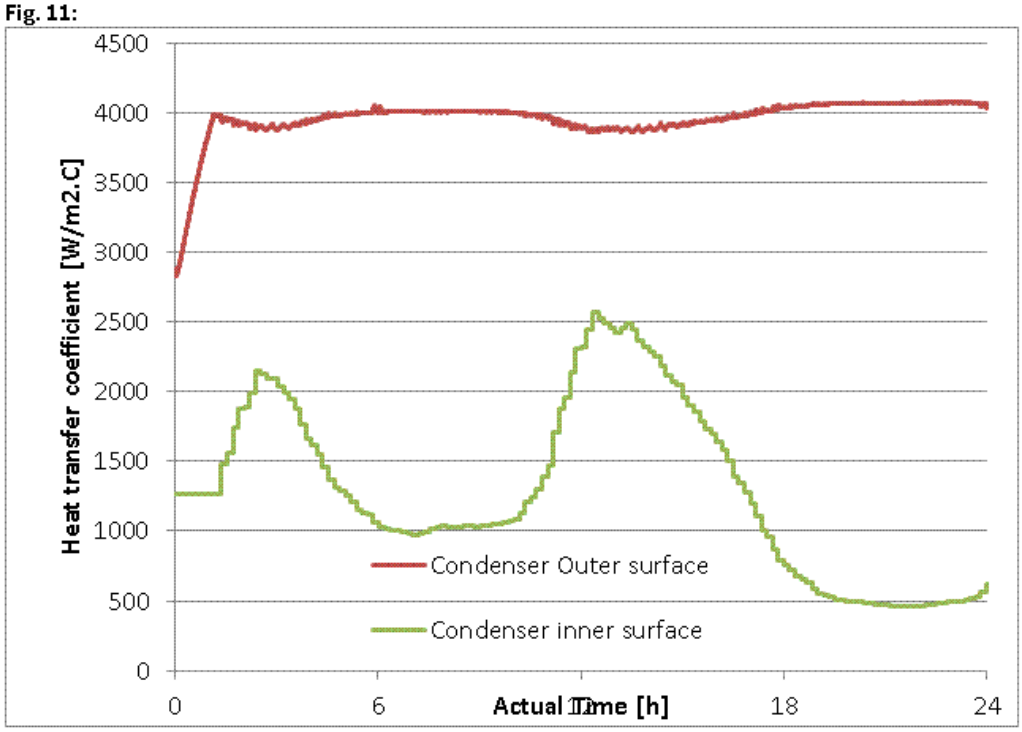

Fig. 12:

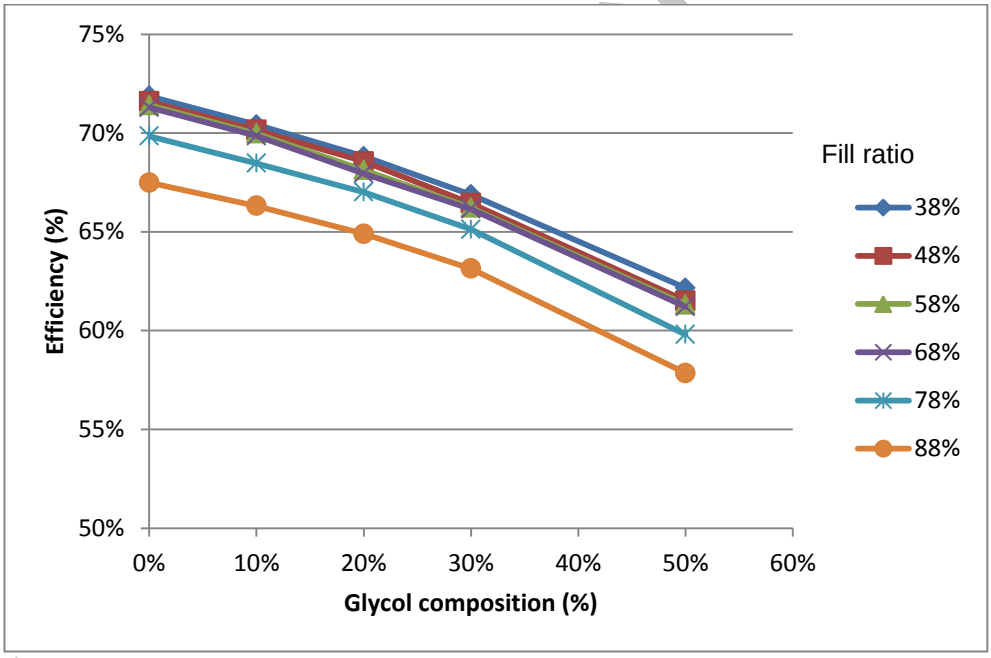

Fig. 13: Effect of working fluid ethylene glycol/water composition on efficiency

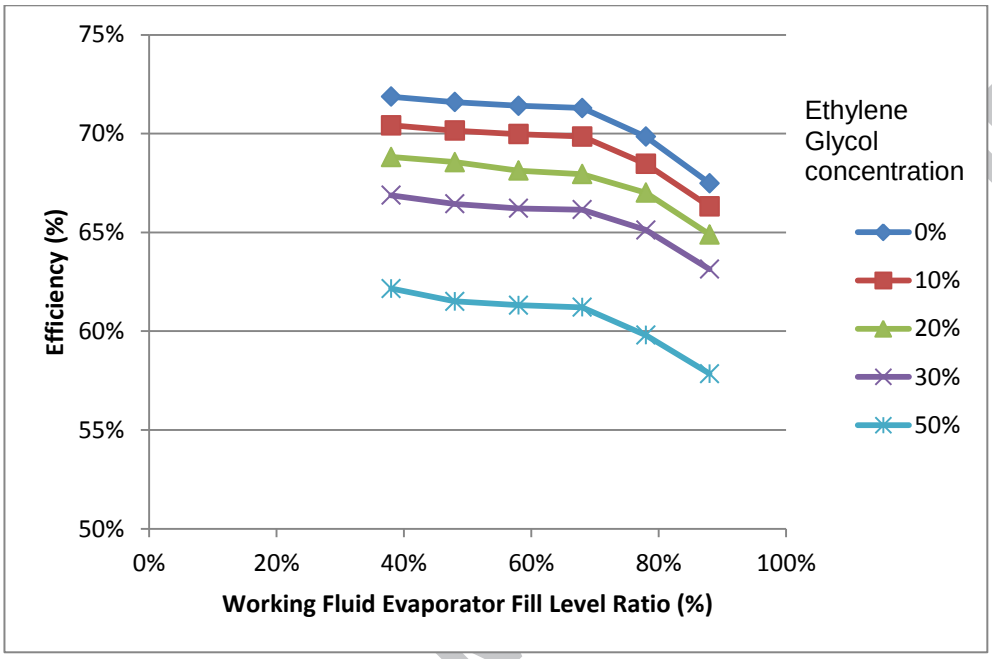

Fig. 14: Effect of filling ratio on efficiency

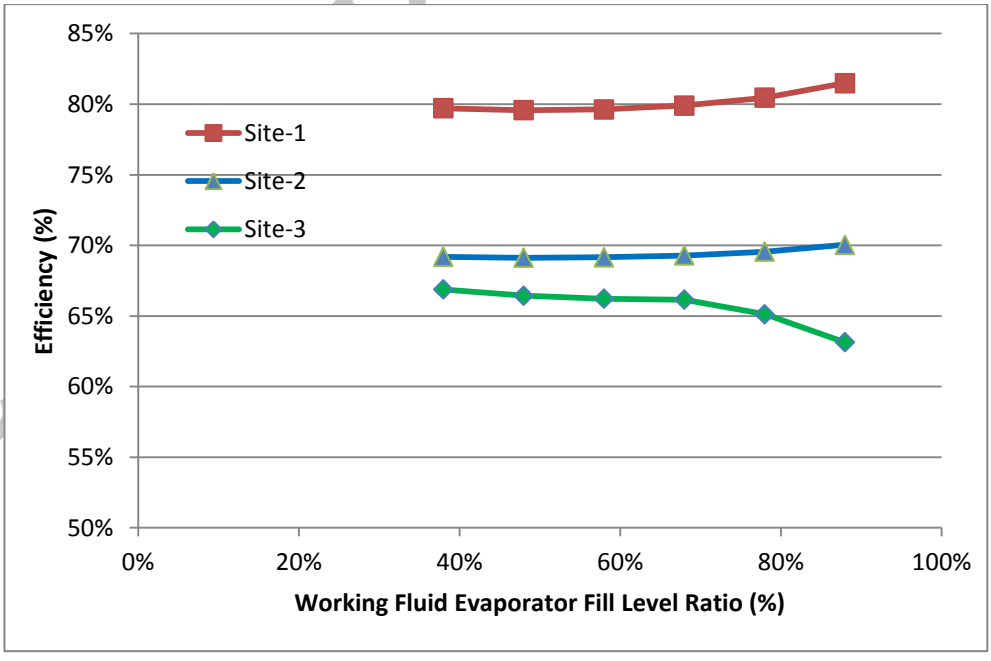

Fig. 15: Effect of filling ratio on efficiency for sites 1 to 3

Highlight:

- A two-phase thermosyphon is proposed to counteract the Joule-Thompson effect.
- A transient numerical model based on lumped capacitance method is used.
- Experimental and numerical data compared.
- Efficiencies between 68% and 80% are estimated.